Complete inhibition of ABCB1 and ABCG2 at the blood–brain barrier by co-infusion of erlotinib and tariquidar to improve brain delivery of the model ABCB1/ABCG2 substrate [11C]erlotinib

Nicolas Tournier[1], Sebastien Goutal[1,2], Severin Mairinger[3] (ID),
Irene Hernández-Lozano[4], Thomas Filip[3], Michael Sauberer[3],
Fabien Caillé[1], Louise Breuil[1], Johann Stanek[3],
Anna F Freeman[5], Gaia Novarino[5], Charles Truillet[1],
Thomas Wanek[3] and Oliver Langer[3,4,6] (ID)

Abstract

P-glycoprotein (ABCB1) and breast cancer resistance protein (ABCG2) restrict at the blood–brain barrier (BBB) the brain distribution of the majority of currently known molecularly targeted anticancer drugs. To improve brain delivery of dual ABCB1/ABCG2 substrates, both ABCB1 and ABCG2 need to be inhibited simultaneously at the BBB. We examined the feasibility of simultaneous ABCB1/ABCG2 inhibition with i.v. co-infusion of erlotinib and tariquidar by studying brain distribution of the model ABCB1/ABCG2 substrate [11C]erlotinib in mice and rhesus macaques with PET. Tolerability of the erlotinib/tariquidar combination was assessed in human embryonic stem cell-derived cerebral organoids. In mice and macaques, baseline brain distribution of [11C]erlotinib was low (brain distribution volume, $V_{T,brain} < 0.3$ mL/cm^3). Co-infusion of erlotinib and tariquidar increased $V_{T,brain}$ in mice by 3.0-fold and in macaques by 3.4- to 5.0-fold, while infusion of erlotinib alone or tariquidar alone led to less pronounced $V_{T,brain}$ increases in both species. Treatment of cerebral organoids with erlotinib/tariquidar led to an induction of Caspase-3-dependent apoptosis. Co-infusion of erlotinib/tariquidar may potentially allow for complete ABCB1/ABCG2 inhibition at the BBB, while simultaneously achieving brain-targeted EGFR inhibition. Our protocol may be applicable to enhance brain delivery of molecularly targeted anticancer drugs for a more effective treatment of brain tumors.

Keywords

Blood–brain barrier, P-glycoprotein, breast cancer resistance protein, brain delivery, transporter inhibition

[1]Laboratoire d'Imagerie Biomédicale Multimodale (BioMaps), Université Paris-Saclay, CEA, CNRS, Inserm, Service Hospitalier Frédéric Joliot, Orsay, France
[2]MIRCen, CEA/IBFJ/DRF-JACOB/LMN, UMR CEA CNRS 9199-Université Paris Saclay, Fontenay-aux-Roses, France
[3]Preclinical Molecular Imaging, AIT Austrian Institute of Technology GmbH, Seibersdorf, Austria
[4]Department of Clinical Pharmacology, Medical University of Vienna, Vienna, Austria
[5]Institute of Science and Technology (IST) Austria, Klosterneuburg, Austria
[6]Department of Biomedical Imaging und Image-guided Therapy, Division of Nuclear Medicine, Medical University of Vienna, Vienna, Austria

Corresponding authors:
Nicolas Tournier, CEA/SHFJ, 4 Place du Général Leclerc, Orsay 91400, France.
Email: nicolas.tournier@cea.fr
Oliver Langer, Preclinical Molecular Imaging, AIT Austrian Institute of Technology, GmbH, Seibersdorf 2444, Austria.
Email: oliver.langer@ait.ac.at

Introduction

Despite great progress in the design of brain-penetrant, small-molecule therapeutics, the achievement of high and prolonged central nervous system (CNS) exposure of drug molecules still remains a major challenge, in particular for certain drug classes, such as molecularly targeted anticancer drugs.[1] One important reason for low and sub-therapeutic CNS exposure is efflux transport by P-glycoprotein (ATP-binding cassette subfamily B member 1, ABCB1) and breast cancer resistance protein (ATP-binding cassette subfamily G member 2, ABCG2). These two transporters are co-localized in the luminal (blood-facing) membrane of brain capillary endothelial cells which are part of the blood–brain barrier (BBB).[2] They possess an exceptionally broad and largely overlapping substrate spectrum and act as gatekeepers in preventing the brain entry of many small-molecule drugs.[3,4] Moreover, there is ample evidence for functional redundancy between ABCB1 and ABCG2 at the BBB, i.e. in absence of either ABCB1 activity or ABCG2 activity (e.g. due to genetic knock-out or pharmacological transporter inhibition), the remaining transport capacity of the other transporter often suffices to largely restrict CNS exposure of shared (dual) ABCB1/ABCG2 substrate drugs.[3–5] Although major efforts have focused on the design of molecularly targeted anticancer drugs with lack of or diminished ABCB1/ABCG2 efflux liability, this endeavor has only been successful in certain cases (e.g. osimertinib, AZD3759).[6–8] The majority of currently known and newly developed molecularly targeted anticancer drugs is hindered from entering the brain by ABCB1/ABCG2 efflux.[3,4,9] This most often results in lack of efficacy for the treatment of primary or secondary brain tumors, for which a desperate and unmet medical need exists.

The pharmacological inhibition of ABCB1 and ABCG2 has been proposed as a strategy to improve brain access of dual ABCB1/ABCG2 substrate drugs.[9,10] Such an approach may not be without risks, as off-target inhibition of ABCB1 and ABCG2 in other organs than the brain, such as excretory organs or the bone marrow, may lead to unwanted side effects and toxicity. Nevertheless, in absence of other effective therapies, such risks may be justified in case of hospitalized, terminally ill patients, for whom controlled transporter inhibition at the BBB may be a viable option for improved treatment of CNS malignancies.

Building on earlier experience with agents developed for the reversal of tumor multidrug resistance,[11,12] several academic research groups have attempted to repurpose these agents for effective transporter inhibition at the BBB. From these efforts, two third-generation transporter inhibitors have emerged as promising agents, i.e. tariquidar and elacridar. While tariquidar mainly achieves ABCB1 (and not ABCG2) inhibition at clinically feasible doses[13,14] and is therefore considered unsuitable to significantly enhance the brain distribution of dual ABCB1/ABCG2 substrates in humans,[15,16] elacridar appears to be equipotent in inhibiting ABCB1 and ABCG2. Several preclinical studies showed that elacridar can effectively increase brain penetration of dual ABCB1/ABCG2 substrates,[3] such as the epidermal growth factor receptor (EGFR)-targeted tyrosine kinase inhibitor erlotinib.[17–19] However, elacridar possesses very low oral bioavailability in humans, so that plasma concentrations attained after oral administration were far below the concentrations needed to inhibit ABCB1 and ABCG2 at the human BBB.[20] We have recently shown that continuous intravenous (i.v.) infusion of elacridar can inhibit ABCB1 and ABCG2 at the BBB of non-human primates (NHPs) and increase in *Papio anubis* baboons brain concentrations of [11C]erlotinib, measured with positron emission tomography (PET), to similar levels as muscle tissue surrounding the skull, which points to complete transporter inhibition at the BBB.[18] However, elacridar has very poor water solubility and formulation of the drug for i.v. administration required unacceptably high concentrations of organic solvent (tetrahydrofuran) for human use.[21] In comparison to elacridar, tariquidar possesses better water solubility and can be formulated for i.v. administration in a solvent suitable for human use.[13–15,22,23] PET studies in healthy volunteers showed that tariquidar at i.v. doses up to 6 mg/kg is well tolerated and leads to 4- to 5-fold increases in the brain penetration of the model ABCB1 substrates (R)-[11C]verapamil and [11C]N-desmethyl-loperamide.[13,14,22,23] Erlotinib is a potent ABCG2 inhibitor[24,25] and we have shown that single-dose oral administration of high-dose erlotinib (650 mg) significantly increased the brain penetration of [11C]erlotinib in healthy volunteers, although inhibition/saturation of efflux transport at the BBB was not maximal.[16] We hypothesize that a combination of erlotinib and tariquidar may overcome the limitations of tariquidar, elacridar or erlotinib and provide a clinically feasible strategy to achieve complete inhibition of both ABCB1 and ABCG2 at the BBB resulting in increased brain penetration of ABCB1/ABCG2 substrate drugs, while simultaneously achieving EGFR inhibition in the brain.

In the present work, we used PET imaging with [11C]erlotinib in mice and NHPs (*Macaca mulatta*) to examine the feasibility of dual ABCB1 and ABCG2 inhibition with a combination of erlotinib and tariquidar. Moreover, the tolerability of combined treatment with erlotinib/tariquidar was assessed in human embryonic stem cell (hESC)-derived cerebral organoids.

Material and methods

Chemicals and drugs

Unless otherwise stated, all chemicals were purchased from Sigma-Aldrich (Schnelldorf, Germany) or Merck (Darmstadt, Germany). Tariquidar dimesylate was purchased from Haoyuan Chemexpress Co., Ltd (Shanghai, PRC) or from Eras Labo (Saint-Nazaire-Les-Eymes, France). Erlotinib hydrochloride was purchased from Apollo Scientific (Bredbury, UK). Captisol® was obtained from Cydex Pharmaceuticals or Ligand Pharmaceuticals, Inc. (San Diego, CA, USA). For in vitro experiments in cerebral organoids, stock solutions of tariquidar dimesylate (5 mg/mL) and erlotinib hydrochloride (10 mg/mL) in DMSO were prepared.

Radiotracer synthesis

[^{11}C]Erlotinib was synthesized as described elsewhere.[26] For i.v. injection into mice, [^{11}C]erlotinib was formulated in 0.1 mM hydrochloric acid in physiological saline (0.9%, w/v). Molar activity at the time of injection was 73 ± 29 GBq/µmol ($n = 26$) and radiochemical purity was >98%. For experiments in macaques, [^{11}C]erlotinib was formulated in 0.9% aqueous saline with 10% ethanol (v/v). The radiochemical purity of [^{11}C]erlotinib was >98% and the molar activity at the time of injection was 22 ± 3 GBq/µmol ($n = 6$).

Animals

Female Friend leukemia virus B (FVB) mice were obtained from Charles River (Sulzfeld, Germany). At the time of experiment, animals were 7–15 weeks old and weighed 23.1 ± 1.6 g. In total, 26 mice were used in the experiments and each animal was used for only one PET scan. All animals were housed in type III IVC cages under controlled environmental conditions (21.8 ± 1.0°C, 40% to 70% humidity, 12-h light/dark cycle) with free access to standard laboratory rodent diet (LASQCdiet^{TM}, LASvendi, Soest, Germany) and water. An acclimatization period of at least 1 week was allowed before the animals were used in the experiments. The study was approved by the national authorities (Amt der Niederösterreichischen Landesregierung) and study procedures were in accordance with the European Communities Council Directive of 22 September 2010 (2010/63/EU).

Experiments in NHPs were conducted using two adult male rhesus macaques (*Macaca mulatta*; weight M1: 8.77 ± 0.74 kg and M2: 13.54 ± 0.84 kg during the course of the study) obtained from Silabe, France. A minimum interval of two weeks was respected between two scans in the same monkey to allow for complete recovery. Animal use procedures were in accordance with the recommendations of the European Community for the care and use of laboratory animals (2010/63/EU) and the French National Committees (French Decret 2013-118). The experimental protocol (reference n°17-050) was validated by a local ethics committee for animal use (Comité d'Ethique en Expérimentation Animale, CEtEA-044) and approved by the French government (reference APAFIS N°19200-2017121312309702 v4). The animal experimental data reported in this study are in compliance with the ARRIVE (Animal Research: Reporting in Vivo Experiments) guidelines.

PET imaging in mice

Drug administration protocol. We investigated four groups of mice. (1) One group was treated with vehicle, (2) one group with a bolus injection and continuous infusion of erlotinib, (3) one group with a bolus injection of tariquidar, and (4) one group with a bolus injection and continuous infusion of erlotinib plus a bolus injection of tariquidar. Table 1 gives an overview of examined animal groups and numbers and administered inhibitor doses. Doses of erlotinib and tariquidar were chosen based on previous studies in mice.[27,28] A half-maximum inhibitory concentration (IC$_{50}$) of 1052 nM (corresponding to an i.v. dose of approximately 6 mg/kg) was reported for tariquidar to increase brain uptake of the ABCB1 substrate (R)-[^{11}C]verapamil in mice.[27] In rats, the half-maximum inhibitory dose of tariquidar for ABCB1 was in the same range (3 to 5 mg/kg).[29,30] For i.v. administration, tariquidar dimesylate was dissolved in 2.5% (w/v) aqueous glucose solution. Erlotinib hydrochloride was dissolved in 2.5% (w/v) aqueous glucose solution containing 3% (w/v) Captisol®.

Imaging procedure. Imaging experiments were performed under isoflurane/oxygen anesthesia. Animals were

Table 1. Overview of inhibitor doses, examined mouse groups and numbers.

Inhibitor	Bolus dose (mg/kg)[a]	Infusion (mg/kg/h)[b]	Total dose (mg/kg)[c]	n
Vehicle[d]	–	–	–	10
Erlotinib	8.6	8.6	21.5	4
Tariquidar	10	–	10	4
Erlotinib/tariquidar	8.6/10	8.6/–	21.5/10	8

[a]Given in a volume of 100 µL as an i.v. bolus over 1 min at 30 or 15 min before start of the PET scan.
[b]Given in a volume of 150 µL as an i.v. infusion over 90 min until the end of the PET scan.
[c]Total dose from bolus and continuous infusion.
[d]Total volume 250 µL (100 µL bolus + 150 µL continuous infusion).

warmed throughout the experiment and body temperature (36.5–38.0°C) and respiratory rate (30–60 breaths/s) were constantly monitored. Mice were placed in an imaging chamber (m2m imaging Corp, Cleveland, Ohio, USA) and both lateral tail veins were cannulated for i.v. administration. A microPET Focus220 scanner (Siemens Medical Solutions, Knoxville, TN, USA) was used for PET imaging. At 30 min before start of the PET scan, animals received via one of the catheters erlotinib (8.6 mg/kg) or vehicle solution (total volume: 100 μL) as an i.v. bolus over 1 min followed by a continuous infusion of erlotinib (8.6 mg/kg/h) or vehicle solution until the end of the PET scan (Harvard Apparatus Syringe pump 11 Elite, total duration: 90 min, total volume: 150 μL). At 15 min before start of the PET scan, animals in the tariquidar groups received via the other catheter an i.v. bolus injection (volume: 100 μL) of tariquidar (10 mg/kg) over 1 min. Dynamic emission scans (60 min) were started with the i.v. injection of [^{11}C]erlotinib (27 ± 7 MBq in a volume of 100 μL, corresponding to 0.5 ± 0.2 nmol of unlabeled erlotinib). List-mode data were acquired with a timing window of 6 ns and an energy window of 250–750 keV. At the end of the PET scan, a terminal blood sample was withdrawn from the retro-bulbar plexus and animals were sacrificed by cervical dislocation while still under deep anesthesia and whole brains were removed. Blood was centrifuged to obtain plasma and radioactivity in blood, plasma and brain was measured in a gamma counter (Wizard 1470, Perkin Elmer or Hidex Model#425, Hidex, Turku, Finland). Radioactivity counts were normalized to sample weight, corrected for radioactive decay and used to determine brain-to-blood ($K_{b,brain}$) and brain-to-plasma ($K_{p,brain}$) ratios.

Mouse data analysis. The dynamic PET data were binned into 23 frames, which incrementally increased in time length. PET images were reconstructed using Fourier re-binning of the three-dimensional sinograms followed by a two-dimensional filtered back-projection with a ramp filter giving a voxel size of $0.4 \times 0.4 \times 0.796$ mm^3. Using AMIDE software,[31] whole brain and the left ventricle of the heart (to obtain an image-derived blood curve) were manually outlined on the PET images to derive time-activity curves (TACs) expressed in units of standardized uptake value (SUV = (radioactivity per g/injected radioactivity). body weight). From the brain TACs, the area under the curve from 0 to 60 min (AUC$_{brain}$, SUV.min) was determined as a measure of the brain exposure to [^{11}C]erlotinib. The image-derived blood curve was converted into the corresponding plasma curve by multiplying the blood values with the plasma-to-blood radioactivity ratio measured for each animal in the gamma counter.

Total distribution volume in the brain ($V_{T,brain}$, mL/cm^3) was estimated by performing Logan graphical analysis using the image-derived plasma curve.[32] $V_{T,brain}$ corresponds to the brain-to-plasma ratio of radioactivity at steady state. In addition, integration plot analysis was performed as described previously[28] to estimate the rate constant for initial transfer of radioactivity from plasma into brain ($k_{uptake,brain}$, mL/min/g brain) using data measured from 0.3 min to 1.8 min after radiotracer injection.

PET imaging in non-human primates

Drug administration protocol. Two rhesus macaques underwent [^{11}C]erlotinib PET scans before (baseline) and during infusion of the erlotinib/tariquidar combination. For comparison, one animal received either erlotinib alone or tariquidar alone using infusion protocols, which have been previously used and validated in baboons.[18,33] Doses of erlotinib and tariquidar were selected based on available tolerance data and dose-response data (for tariquidar) obtained from previous work performed in baboons[18,33] and humans.[14,16] Tariquidar solution for i.v infusion (4 mg/kg/h) was prepared on the day of the experiment by dissolving tariquidar dimesylate in a 5% (w/v) glucose solution as described previously.[33] Tariquidar solution was infused at a rate of 6.7 mL/h during 90 min starting 30 min before injection of [^{11}C]erlotinib. Erlotinib solution for i.v infusion (10 mg/kg/h) was prepared on the day of the experiment by dissolving erlotinib hydrochloride in sterile water containing 6% (w/v) Captisol® followed by 1:1 dilution with 5% (w/v) glucose solution.[18] The erlotinib solution was infused at a rate of 20 mL/h during 120 min, starting 60 min before injection of [^{11}C]erlotinib.

Imaging procedure. PET acquisitions were performed on an HR+ Tomograph (Siemens Healthcare, Knoxville, TN, USA) in anesthetized animals in supine position under suitable monitoring as described previously.[18] Briefly, the animal received ketamine (10 mg/kg) to induce anesthesia. Once the animal was intubated, venous catheters were inserted for radiotracer injection (sural vein), propofol infusion (sural vein) and drug injection (right or left brachial vein or both for combined erlotinib/tariquidar infusion). Another catheter was inserted into the femoral artery for arterial blood sampling. The animal was positioned under the camera before administration of a 2 mL i.v. bolus of propofol (Aspen Pharma, Paris, France) followed by a 1 mL/kg/h i.v. infusion under oxygen ventilation. Animals were injected i.v. with [^{11}C]erlotinib (228 ± 19 MBq in a volume of 5 mL, corresponding to 10.3 ± 1.6 nmol of unlabeled erlotinib). A dynamic PET acquisition

(60 min) in three-dimensional mode was then started to measure the brain kinetics of [^{11}C]erlotinib. Animals were extubated approximately 15 min after end of PET scanning. Animals were then continuously monitored for at least 60 min.

Arterial input function and metabolism. During PET acquisition, arterial blood samples (approximately 0.2 mL) were withdrawn for assessment of the arterial input function of total radioactivity. Blood samples were centrifuged and counted using a calibrated gamma-counter (Cobra, Perkin-Elmer, France). Additional plasma samples (0.5 mL) were collected at 0, 5, 10, 15, 30 and 60 min after radiotracer injection to estimate the percentage of unmetabolized [^{11}C]erlotinib by radio-high performance liquid chromatography analysis as described previously.[18] For each animal, a 1-exponential decay function was fitted to the percentage of unmetabolized [^{11}C]erlotinib *versus* time and then applied to the corresponding total radioactivity TAC in plasma. TACs of unmetabolized [^{11}C]erlotinib in plasma were expressed in SUV units *versus* time. Unmetabolized [^{11}C]erlotinib plasma exposure was estimated under all tested conditions by calculating the AUC from 0 to 60 min.

Non-human primate data analysis. Measured attenuation and scatter corrections were applied to the emission data. Data were reconstructed using the 3D reprojection algorithm with an axial and transaxial Hanning filter with the cutoff set to the Nyquist frequency. Image analysis was performed using PMOD® software (version 3.8, PMOD Technologies Ltd, Zürich, Switzerland). For each animal, summed PET images were co-registered to previously acquired T1-weighted brain magnetic resonance images. The whole brain and temporal muscle surrounding the skull were outlined and applied to dynamic PET images to generate TACs. Brain and muscle tissue exposure was estimated as the AUC from 0 to 60 min. The BBB penetration of [^{11}C]erlotinib was estimated either as the brain-to-plasma AUC ratio ($AUCR_{brain/plasma}$) or as the brain-to-muscle AUC ratio ($AUCR_{brain/muscle}$), assuming negligible ABC transporter activity at the blood–muscle interface.[34] Moreover, kinetic modeling was performed using Logan plot analysis with the corresponding metabolite-corrected arterial plasma input function to estimate $V_{T,brain}$.[32] Compartmental models (1- or 2-tissue compartment) did not provide accurate estimates of outcome parameters to describe the brain kinetics of [^{11}C]erlotinib. Therefore, integration plot analysis was used as for the mouse data to estimate $k_{uptake,brain}$ (mL/min/g brain) using data measured from 0.75 min to 3 min after radiotracer injection.[28]

Human embryonic stem cell-derived cerebral organoids

Multicell cerebral organoids of hESCs were cultivated in StemFlex media for 60 days.[35] The hESCs were seeded into 6-well plates coated with matrigel. After three days, cells were dissociated into single cells and seeded into 96 ultra-low attachment plates for the next three to four days to form an embryonic body. At the size of 420 μm, they were induced with neural induction media. After several rounds of neural inductions, generated embryonic bodies with large and more continuous neuroepithelium were embedded into matrigel droplets on a sheet of Parafilm with small 3 mm dimples. These droplets were allowed to gel at 37°C, removed from the Parafilm and grown in differentiation media containing a 1:1 mixture of DMEM/F12 and Neurobasal containing 1:200 N2 supplement (Invitrogen), 1:100 B27 supplement without vitamin A (Invitrogen), 3.5 μL 2-mercaptoethanol, 1:4000 insulin (Sigma), 1:100 Glutamax (Invitrogen) and 1:200 MEM-NEAA. After four days of stationary growth, the droplets were transferred to an orbitary shaker (65 rpm/min) containing differentiation media as above, except that B27 supplement with vitamin A (Invitrogen) was used; 60-days-old organoids (one organoid per treatment) were incubated at 37°C (5% CO_2, 95% humidity) for 24 h in media with 0.1% DMSO (DMSO control), erlotinib hydrochloride (10 μg/mL), tariquidar dimesylate (5 μg/mL) and a combination of erlotinib hydrochloride (10 μg/mL) and tariquidar dimesylate (5 μg/mL).

Cryostat sectioning of cerebral organoids. After incubation, organoids were fixed with 4% paraformaldehyde and soaked in 30% sucrose solution for three days. After the fixation step, they were embedded in O.C.T and frozen on dry ice. The frozen cerebral organoids were cryosectioned at −20°C using a Microm HM 560 cryostat (Thermo Scientific) to provide slices with a thickness of 18 μm.

Anti-active caspase-3 immunostaining. The cryosectioned slices (eight slices per cerebral organoid) were dried at room temperature for 2 h and Heat-Induced Epitope Retrieval with Dako Target Retrieval Solution was performed to increase the accessibility of antigen and the staining intensity. The retrieval procedure involves immersion of tissue sections mounted on slides in diluted Target Retrieval Solution and heating in a water bath at 95°C. The sections were blocked and permeabilized in 2% of normal donkey serum and 0.3% triton-X100. The slides were incubated with Caspase-3 antibody (Cell Signaling Technology, Inc., Danvers, MA, USA, Rabbit polyclonal, 9662) overnight at 4°C.

After 24 h incubations, they were washed three times with phosphate-buffered saline and incubated with Hoechst 33342 dye (Invitrogen) and finally secondary anti-Rabbit antibody.

Imaging. The stained cryosections were imaged at 4× magnification by using an Axio Scan.Z1 slide scanner (Carl Zeiss Microscopy GmbH, Jena, Germany). Positive cells were counted in each region of interest using ImageJ software.

Statistical analysis

All values are either given as mean ± standard deviation (SD) or as individual values. Statistical testing was performed using Prism 8.0 software (GraphPad Software, La Jolla, CA, USA). After confirmation of the normal distribution of the data using the Shapiro–Wilk normality test, differences in outcome parameters between groups were tested with one-way ANOVA with Dunnett's multiple comparisons test. To assess correlations, the Pearson correlation coefficient r was calculated. The level of statistical significance was set to a p value of less than 0.05.

Results

Mouse experiments

We investigated groups of mice, which were administered vehicle solution, erlotinib alone, tariquidar alone or a combination of erlotinib and tariquidar (Table 1). As outcome parameters for the brain exposure and BBB penetration of [11C]erlotinib, we determined AUC_{brain}, $V_{T,brain}$ and $k_{uptake,brain}$. For the determination of $V_{T,brain}$ and $k_{uptake,brain}$, the TACs in arterial plasma were required. Arterial blood curves were derived from the PET images by placing a region of interest into the left ventricle of the heart. Blood radioactivity concentrations derived from the last PET frame showed a good correlation with radioactivity concentrations measured with a gamma counter in a venous blood sample collected at the end of the PET scan ($r = 0.814$, $p < 0.0001$, slope $= 1.67 \pm 0.27$). In the two animal groups which received erlotinib, total plasma radioactivity concentrations measured at the end of the PET scan in the gamma counter were significantly higher than in the vehicle group (Figure 1(a)). In Figure 1(b), TACs in the brain are shown for all groups. Brain TACs were low in the vehicle and erlotinib groups, on an intermediate level in the tariquidar group and highest in the erlotinib/tariquidar group. AUC_{brain} and $V_{T,brain}$ values in individual animals per group are shown in Figure 1(c) and (d) and $k_{uptake,brain}$ values are shown in Supplementary Figure 1. In

agreement with the brain TACs, all three parameters were comparably low for the vehicle and erlotinib groups, intermediate for the tariquidar group and highest in the erlotinib/tariquidar group. AUC_{brain} was significantly increased by 2.0-fold in the tariquidar group and by 3.8-fold in the erlotinib/tariquidar group, as compared with the vehicle group (Figure 1(c)). For comparison, $Abcb1a/b^{(-/-)}Abcg2^{(-/-)}$ mice, which had been examined in a previous study,[17] had a 1.9-fold higher AUC_{brain} than the vehicle group. This discrepancy in AUC_{brain} between $Abcb1a/b^{(-/-)}Abcg2^{(-/-)}$ mice and erlotinib/tariquidar-treated wild-type-mice may be related to higher plasma radioactivity exposure in the latter. $V_{T,brain}$, which takes plasma radioactivity concentrations into account, was 1.9-fold higher in the tariquidar group, 3.0-fold higher in the erlotinib/tariquidar group and 2.1-fold higher in $Abcb1a/b^{(-/-)}Abcg2^{(-/-)}$ mice as compared with the vehicle group (Figure 1(d)). As an additional measure of the brain distribution of [11C]erlotinib, we determined $K_{b,brain}$ and $K_{p,brain}$ from samples collected from the animals after the PET scan (Supplementary Figure 2). $K_{b,brain}$ and $K_{p,brain}$ values followed a similar trend as AUC_{brain}, $V_{T,brain}$ and $k_{uptake,brain}$ with low values in the vehicle and erlotinib groups, intermediate values in the tariquidar group and highest values in the erlotinib/tariquidar group.

Non-human primate experiments

We assessed in two rhesus macaques the effect of combined infusion of erlotinib and tariquidar on the brain distribution of [11C]erlotinib in comparison with control animals, which received no treatment (baseline). In addition, one animal each was either treated with erlotinib or with tariquidar infusion alone. All treatments were well tolerated and neither a change in pCO_2, heart rate, rectal temperature nor respiratory frequency was observed during and after infusion. PET summation images for all tested conditions are shown in Figure 2 and TACs in arterial plasma, brain and muscle are shown in Figure 3. Similar to the mouse data (Figure 1(b)), brain [11C]erlotinib concentrations were highest in the erlotinib/tariquidar group and comparable to baseline in the erlotinib group (Figure 3(b)). In contrast to the mouse data, tariquidar infusion alone produced no effect on the brain concentrations of [11C]erlotinib in the single examined animal. Erlotinib/tariquidar infusion changed the kinetics and increased the level of exposure of [11C]erlotinib in arterial plasma (Figure 3(a)) and muscle tissue (Figure 3(c)). In Table 2, pharmacokinetic parameters are given for all investigated conditions. Erlotinib/tariquidar co-infusion induced a 3.9- and 5.6-fold increase in AUC_{brain} in the two examined animals. There was
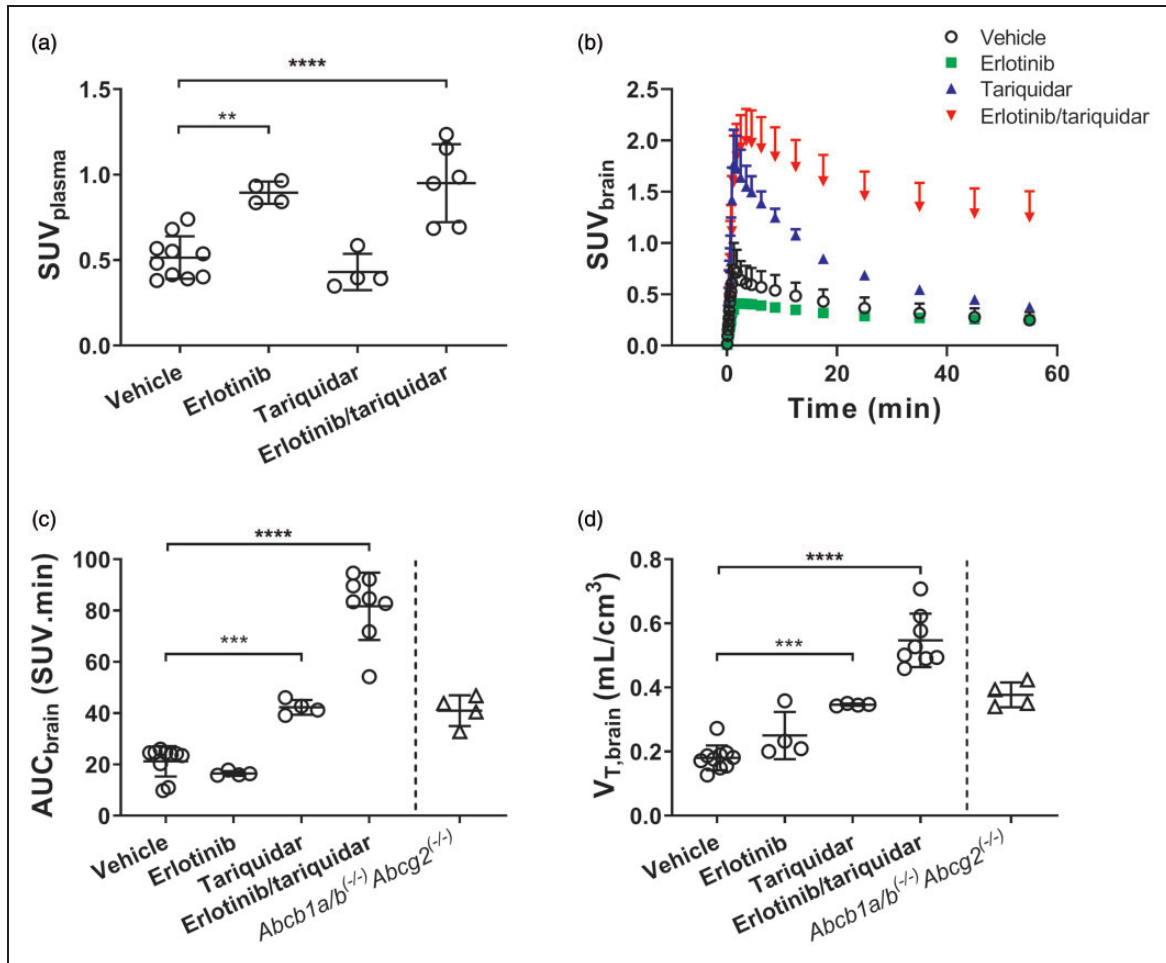
**Figure 1.** Kinetics of [^{11}C]erlotinib in mice. Total radioactivity concentration in venous plasma collected at the end of the PET scan, measured in a gamma counter in all examined mouse groups (a). Time-activity curves (mean $\pm$ SD) in whole brain (b), AUC$_{brain}$ values (c) and $V_{T,brain}$ values (d) for all examined mouse groups. For comparison, AUC$_{brain}$ and $V_{T,brain}$ values are also shown for $Abcb1a/b^{(-/-)}Abcg2^{(-/-)}$ mice measured in a previous study.[17] $**p < 0.01$; $***p < 0.001$; $****p < 0.0001$, one-way ANOVA with Dunnett's multiple comparisons test.

also a substantial but less pronounced increase (1.7- and 1.4-fold) in AUC$_{muscle}$, which suggested a change in the peripheral kinetics of [^{11}C]erlotinib. $V_{T,brain}$, which takes a change in plasma kinetics into account, was increased by 3.4- and 5.0-fold during erlotinib/tariquidar co-infusion as compared with baseline, consistent with a 2.7-fold-increase in $k_{uptake,brain}$ (Table 2). These results were also consistent with the increases observed in AUCR$_{brain/plasma}$ and AUCR$_{brain/muscle}$, which were used as additional parameters to describe the brain uptake relative to peripheral tissues. In the heavier macaque (M2), brain exposure reached similar levels as muscle exposure resulting in an AUCR$_{brain/muscle}$ value close to 1 (Table 2). The effect of either erlotinib or tariquidar infusion alone on the brain distribution of [^{11}C]erlotinib was less pronounced

suggesting only partial inhibition of ABC transporters, consistent with the data obtained in mice.

Experiments in hESC-derived cerebral organoids

We used hESC-derived cerebral organoids to recapitulate the impact of prolonged exposure to tested inhibitors on human brain cells, in the absence of any BBB efflux transport. Cerebral organoids were treated for 24 h with clinically relevant concentrations of either erlotinib alone (10 µg/mL, 25 µM) or tariquidar alone (5 µg/mL, 6 µM) or a combination of both drugs and Caspase-3 activation was measured as a marker of apoptosis (Figure 4). Treatment with either erlotinib alone or tariquidar alone resulted in no significant changes in Caspase-3 activation compared to the DMSO control
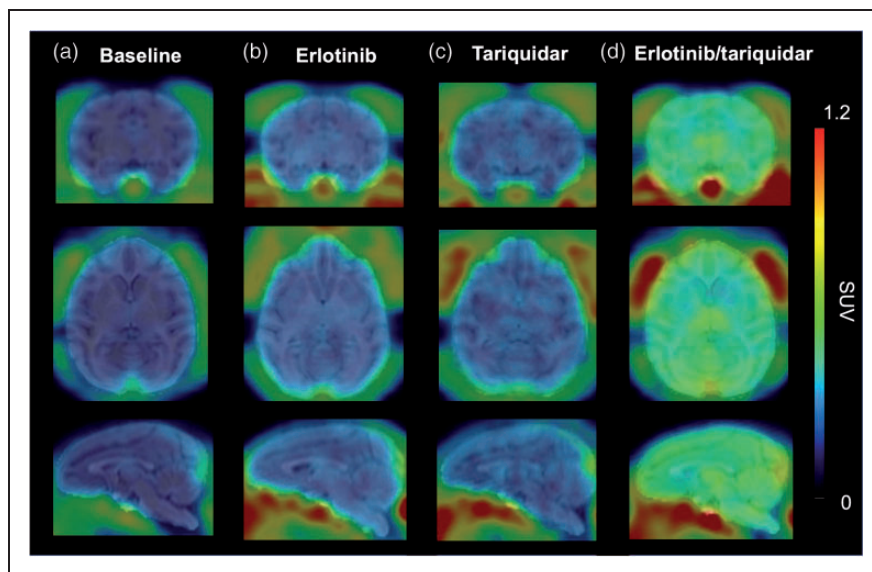
Figure 2. [^{11}C]Erlotinib PET images in nonhuman primate. Representative coronal, axial and sagittal [^{11}C]erlotinib PET summation images (0–60 min) obtained in macaques without (a) or with treatment with erlotinib infusion alone (b), tariquidar infusion alone (c) or combined erlotinib/tariquidar infusion (d).

group. However, the combined treatment with erlotinib and tariquidar resulted in a significant rise in Caspase-3 activation, accounting for $312 \pm 180\%$ of DMSO control (Figure 4). In Supplementary Figure 3, representative stained sections prepared from all groups are shown.

Discussion

The aim of this study was to develop a clinically feasible protocol to achieve complete inhibition of both ABCB1 and ABCG2 activity at the BBB, thus providing a method to improve the brain delivery of dual ABCB1/ABCG2 substrates and enable molecularly targeted therapy of CNS diseases.[9,10] We hypothesized that combined administration of erlotinib and tariquidar, which has each previously been applied as transporter inhibitor in an experimental setting in healthy human volunteers,[14–16] may provide a more effective strategy to inhibit ABCB1 and ABCG2 activity at the BBB than each compound administered alone.

We used PET imaging with [^{11}C]erlotinib as a model ABCB1/ABCG2 substrate to evaluate this novel pharmacological inhibition protocol in mice and NHPs, in a translational approach. A wealth of preclinical and clinical studies, including the use of transporter-deficient mice, have either used unlabeled erlotinib or [^{11}C]erlotinib as prototypical probe substrates to study the importance of ABCB1/ABCG2 activity at the BBB and to increase the extremely low baseline brain penetration of this drug with different pharmacological

inhibition strategies.[5,8,16–20,28,36–38] Combined efflux by ABCB1 and ABCG2, rather than physical integrity of the BBB, was shown to be the rate-limiting factor for the brain delivery of [^{11}C]erlotinib.[17,37]

The main finding of our study is a substantial increase in brain exposure (AUC_{brain}) and BBB penetration ($V_{T,brain}$ and $k_{uptake,brain}$) of [^{11}C]erlotinib in mice and rhesus macaques receiving a co-infusion of erlotinib and tariquidar, while infusion of each drug alone proved to be less effective. The erlotinib/tariquidar combination increased $V_{T,brain}$ in wild-type mice to similar levels as in $Abcb1a/b^{(-/-)}Abcg2^{(-/-)}$ mice, suggesting complete inhibition of ABCB1/ABCG2-mediated efflux at the mouse BBB. In the two macaques treated with the erlotinib/tariquidar combination, $V_{T,brain}$ was increased by 3.4- and 5.0-fold, respectively. The increases in $V_{T,brain}$ induced by the erlotinib/tariquidar combination were more pronounced than the 2.7-fold increase in $k_{uptake,brain}$ measured in the same animals. This suggests that the impact of ABC transporters on the overall brain distribution of [^{11}C]erlotinib may not only be restricted to the initial transfer from plasma into brain across the BBB.[33] In absence of transporter-deficient NHPs, the extent of ABCB1/ABCG2 inhibition was estimated by the $AUCR_{brain/muscle}$ value. The muscle is not protected by ABCB1 and ABCG2 and muscle surrounding the skull has been proposed as a reference region to investigate ABC transporter activity at the BBB, thereby taking any change in peripheral kinetics and/or binding to plasma proteins into account.[34] In our previous study
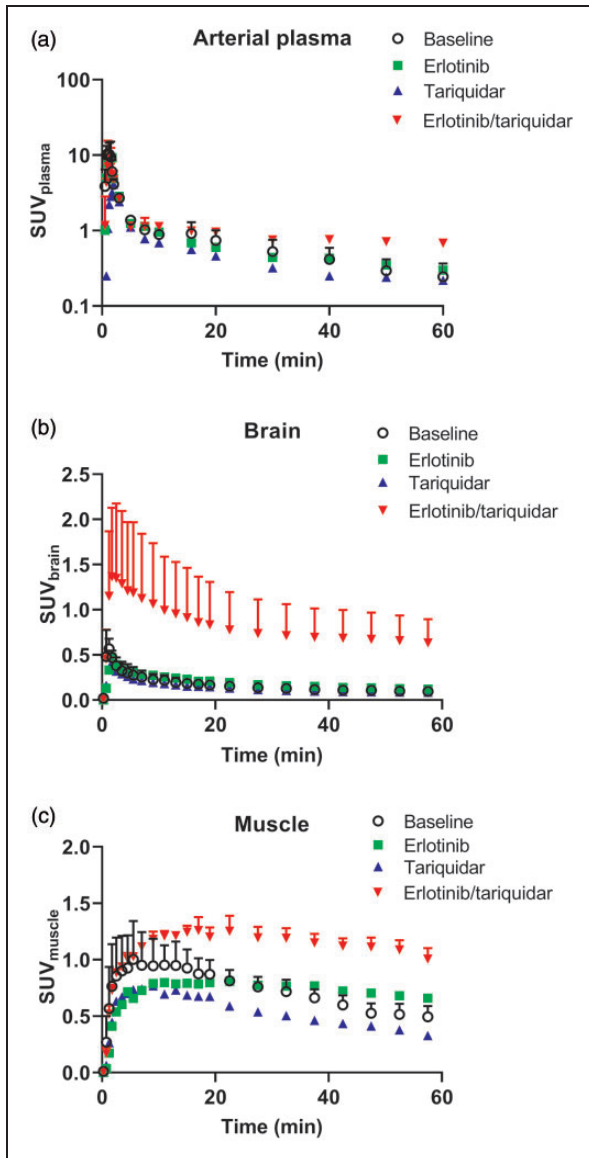
Figure 3. Kinetics of [^{11}C]erlotinib in nonhuman primates. Metabolite-corrected arterial input function of parent [^{11}C]erlotinib in arterial plasma (a) and time-activity curves in the brain (b) and muscle tissue surrounding the brain (c) in macaques under the different tested conditions. Data are presented as individual values or mean ± SD ($n = 2$).

conducted in baboons, infusion of high-dose elacridar increased AUCR$_{brain/muscle}$ of [^{11}C]erlotinib to approximately unity suggesting complete inhibition of efflux transporter activity at the BBB.[18] In the present study, AUCR$_{brain/muscle}$ measured in the two macaques treated with the erlotinib/tariquidar combination was 0.5 and 1, which corresponded to a 2.3- and 4.0-fold increase over baseline, respectively. This suggested that complete inhibition of ABC transporter-mediated efflux of [^{11}C]erlotinib was achieved in the animal

which received the higher absolute dose of erlotinib and tariquidar.

In both mice and macaques, co-infusion of erlotinib/tariquidar increased the plasma concentrations of radioactivity, suggesting a change in peripheral pharmacokinetics. Moreover, erlotinib/tariquidar-treated macaques showed a trend towards decreased elimination of [^{11}C]erlotinib from plasma as compared with the control group. Similar effects have been reported in humans treated with high-dose oral erlotinib, which has been attributed to decreased hepatic clearance of [^{11}C]erlotinib caused by inhibition/saturation of hepatic transporters.[39] The change in plasma pharmacokinetics in erlotinib/tariquidar-treated macaques was consistent with the observed increase in radioactivity in the muscle. However, kinetic modeling, which takes the plasma kinetics into account, confirmed that the change in the peripheral kinetics of [^{11}C]erlotinib observed in mice and macaques treated with the erlotinib/tariquidar combination was not the main cause for the increased brain exposure to [^{11}C]erlotinib. It cannot be excluded that the employed inhibitors changed the plasma-free fraction of [^{11}C]erlotinib, which could have influenced the extent of its BBB penetration. However, the plasma-free fraction of [^{11}C]erlotinib cannot be reliably estimated as [^{11}C]erlotinib is highly bound to plasma proteins (>98%).

In mice and macaques treated with the erlotinib/tariquidar combination, the magnitude of the increase in brain distribution of [^{11}C]erlotinib over baseline was compared to animals treated with the same doses of erlotinib or tariquidar alone. It is noteworthy that erlotinib alone did not significantly increase the brain distribution of [^{11}C]erlotinib in mice. In contrast, in *Papio anubis* baboons infusion of high-dose erlotinib alone (10 mg/kg/h) was previously shown to partially inhibit transporter-mediated efflux of [^{11}C]erlotinib at the BBB and increase $V_{T,brain}$ by 1.7-fold,[18] which was confirmed in the single macaque examined in this study. Tariquidar alone markedly increased the brain distribution of [^{11}C]erlotinib in mice but had only a relatively small effect in the examined macaque, consistent with previous data showing that tariquidar alone did not improve the brain penetration of [^{11}C]erlotinib in humans.[16] These discrepancies can be most likely attributed to species differences in the abundance of ABCB1 and ABCG2 at the BBB between rodents (i.e. mice or rats) and NHPs. Proteomic studies have shown that ABCG2 is the predominant efflux transporter at the BBB of cynomolgus monkeys (*Macaca fascicularis*) and humans and that the abundance of ABCG2 is 3.6-fold higher in cynomolgus monkeys than in mice.[40,41] Conversely, ABCB1 abundance in cynomolgus monkeys was only 0.30-fold of that in mice. Consequently, administration of high-dose erlotinib,

Table 2. Impact of investigated treatments on the plasma and tissue kinetics of [^{11}C]erlotinib in NHPs.

Condition	Monkey	AUC$_{plasma}$[a] (SUV.min)	AUC$_{brain}$ (SUV.min)	AUC$_{muscle}$ (SUV.min)	AUCR$_{brain/muscle}$ (unitless)	AUCR$_{brain/plasma}$ (unitless)	$k_{uptake,brain}$ (mL/min/g)	V$_{T,brain}$ (mL/cm^3)
Baseline	M1	46.8	7.4	36.1	0.20	0.16	0.012	0.17
	M2	57.1	11.4	47.3	0.24	0.20	0.013	0.24
Erlotinib/tariquidar	M1	69.4	28.8	61.4	0.47	0.41	0.032	0.58
(10 mg/kg/h; 4 mg/kg/h)	M2	55.2	63.8	67.3	0.95	1.16	0.035	1.21
Erlotinib	M1	47.7	10.9	41.5	0.26	0.23	0.016	0.28
(10 mg/kg/h)								
Tariquidar	M2	30.3	7.9	30.5	0.26	0.26	0.015	0.47
(4 mg/kg/h)								

[a]Corrected for radiolabeled metabolites of [^{11}C]erlotinib.
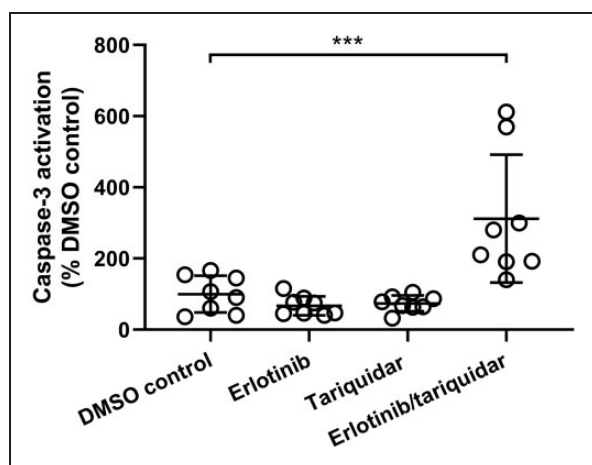
Figure 4. Caspase-3 activation in hESC-derived cerebral organoids. Organoids were incubated for 24 h with medium with 0.1% DMSO (DMSO control), erlotinib hydrochloride (10 μg/mL, erlotinib), tariquidar dimesylate (5 μg/mL, tariquidar) and a combination of erlotinib hydrochloride (10 μg/mL) and tariquidar dimesylate (5 μg/mL) (erlotinib/tariquidar) ($n = 1$ cerebral organoid per treatment with eight slices analyzed per cerebral organoid). Results are expressed as percent of DMSO control. ***$p < 0.001$, one-way ANOVA with Dunnett's multiple comparisons test.

which has a greater potential to inhibit ABCG2,[24] was more effective in inhibiting transporter-mediated efflux of [^{11}C]erlotinib in humans and NHPs than in mice, while tariquidar, which has a greater potential to inhibit ABCB1,[15] was more effective in mice than in humans and NHPs. Therefore, co-infusion of erlotinib and tariquidar may compensate the potential of each single drug for preferentially targeting either ABCB1 or ABCG2, thus enabling more effective inhibition of the overall ABC transporter-mediated efflux of [^{11}C] erlotinib at the BBB. Moreover, this observation strongly supports the use of PET imaging in NHPs to predict the outcome of pharmacological inhibition of ABCB1 and/or ABCG2 at the BBB in humans.[42,43]

Several strategies to overcome ABCB1- and ABCG2-mediated efflux transport at the BBB have been tested in animals but failed to reach clinical application. The dual ABCB1/ABCG2 inhibitor elacridar was successfully translated from rodents to NHPs as a means to improve the brain delivery of erlotinib.[17–19] Unfortunately, the available oral formulation of elacridar for human use did not provide sufficiently high plasma levels of elacridar to improve the brain delivery of [^{11}C]erlotinib in humans.[20] In patients, erlotinib is intended for the oral route. It has been reported that pulsatile dosing of high-dose erlotinib may result in improved disease control in some EGFR-positive non-small cell lung cancer patients with brain metastases.[44] This observation is consistent with an improved brain penetration of [^{11}C]erlotinib enabled by partial inhibition or saturation of ABC transporter-mediated efflux at the BBB by high-dose erlotinib.[16] Given its minimal toxicity, pulsatile erlotinib at a weekly single oral dose of 1000–1500 mg is a reasonable option in patients whose disease has progressed during standard treatment at daily oral doses of 150 mg.[44] Plasma levels achieved during the infusion of 10 mg/kg/h erlotinib in baboons ranged from 5 to 10 μg/mL (13-25 μM),[18] which was in similar range as peak plasma levels measured in patients after pulsatile dosing (15–24 μM for an oral dose of 1600 mg).[45] For comparison, peak erlotinib plasma concentrations after standard clinical dosing (150 mg oral) were reported as 3.7 ± 1.2 μM.[46] Unfortunately, partial and variable clinical response to pulsatile dosing is observed, which may be linked to remaining ABC transporter activity at the BBB, possibly that of ABCB1.[44] Tariquidar can be formulated for i.v. infusion and the dose of tariquidar selected in this work (4 mg/kg/h) has been safely used before in baboons and humans to achieve nearly complete inhibition of ABCB1 activity at the BBB.[14,33] The plasma

levels of tariquidar at this dose were in a similar range in humans $(1.7–4.1\,\mu M)^{14}$ and in baboons $(3.7–6.0\,\mu M)$.[33]

The demonstration of the feasibility and efficacy of erlotinib/tariquidar co-infusion for ABCB1/ABCG2 inhibition at the BBB of NHPs is an important step towards a future translation of this inhibition protocol to humans. A potential advantage of the erlotinib/tariquidar co-infusion protocol is that it not only inhibits ABCB1/ABCG2 activity at the BBB, but may, at the same time, enable CNS-targeted EGFR inhibition and thus allow for the treatment of EGFR-dependent brain tumors or metastases.

Importantly, tariquidar itself is – just like erlotinib – subject to ABCB1- and ABCG2-mediated efflux transport at the BBB.[15,47,48] As a consequence, simultaneous inhibition of ABCB1 and ABCG2 achieved with co-infusion of erlotinib/tariquidar is likely to enhance the brain exposure to both compounds. Increased brain levels of erlotinib alone or tariquidar alone were safely achieved in healthy volunteers.[15,16] However, it is difficult to predict the tolerability of simultaneous high brain exposure to both compounds in humans. Our in vitro data in hESC-derived cerebral organoids, which are not protected by the BBB, showed that erlotinib or tariquidar alone – at concentrations corresponding to the plasma concentrations measured in NHPs – did not induce apoptosis, while there was an apparent synergy between erlotinib and tariquidar in apoptosis induction. Although the exact reasons for this apparent synergy remain unknown, it can be speculated that this was caused by increased intracellular access of erlotinib and/or tariquidar. Caution is therefore warranted to address potential safety issues of the erlotinib/tariquidar combination before a future clinical application in cancer patients. Previous work has shown that the cerebral ABCB1 inhibitory effect of tariquidar in humans is rapidly reversible and only maintained for the duration of the continuous i.v. infusion,[14] so that it can be assumed that only transiently high concentrations of both erlotinib and tariquidar will be achieved in the human brain during application of our inhibition protocol. It is noteworthy that Caspase-3-dependent apoptosis is intended as a therapeutic target and provides an efficacy biomarker for brain-penetrant chemotherapy such as temozolomide.[49,50] Further investigations are therefore needed to address whether apoptosis induced by the erlotinib/tariquidar combination is a limitation for its clinical use or rather a mechanism to potentiate the effects of erlotinib that may help in fighting cancer cells in patients with EGFR-positive CNS tumors or metastases.

Conclusion

We successfully demonstrated in a translational set-up, comprising experiments in mice and NHPs, the efficacy of erlotinib/tariquidar co-infusion to achieve complete inhibition of ABCB1/ABCG2-mediated efflux transport of erlotinib, resulting in substantial increases in its brain exposure and potentially enabling CNS-targeted EGFR inhibition. It remains to be determined whether the erlotinib/tariquidar co-infusion protocol can be combined with other molecularly targeted anticancer drugs and overcome their ABCB1/ABCG2-mediated efflux transport at the BBB, thus allowing a more effective treatment of primary or secondary brain tumors. For a potential future application in cancer patients, particular attention needs to be paid to safety issues.

Declaration of conflicting interests

The author(s) declared no potential conflicts of interest with respect to the research, authorship, and/or publication of this article.

Authors' contributions

Nicolas Tournier, Oliver Langer, Thomas Wanek, Severin Mairinger, Charles Truillet and Gaia Novarino designed the research; Severin Mairinger, Sebastien Goutal, Fabien Caillé, Louise Breuil, Thomas Filip, Michael Sauberer, Johann Stanek and Anna F. Freeman performed the research; Irene Hernández Lozano, Anna F. Freeman, Oliver Langer and Nicolas Tournier analyzed the data; Nicolas Tournier and Oliver Langer wrote the paper.

Supplemental material

Supplemental material for this article is available online.

ORCID iDs

Oliver Langer https://orcid.org/0000-0002-4048-5781
Severin Mairinger https://orcid.org/0000-0001-5094-9351

References

1. Heffron TP. Challenges of developing small-molecule kinase inhibitors for brain tumors and the need for emphasis on free drug levels. *Neuro Oncol* 2018; 20: 307–312.

2. Abbott NJ, Patabendige AA, Dolman DE, et al. Structure and function of the blood-brain barrier. *Neurobiol Dis* 2010; 37: 13–25.

3. Durmus S, Hendrikx JJ and Schinkel AH. Apical ABC transporters and cancer chemotherapeutic drug disposition. *Adv Cancer Res* 2015; 125: 1–41.

4. Agarwal S, Hartz AM, Elmquist WF, et al. Breast cancer resistance protein and P-glycoprotein in brain cancer: two gatekeepers team up. *Curr Pharm Des* 2011; 17: 2793–2802.

5. Kodaira H, Kusuhara H, Ushiki J, et al. Kinetic analysis of the cooperation of P-glycoprotein (P-gp/Abcb1) and breast cancer resistance protein (bcrp/Abcg2) in limiting the brain and testis penetration of erlotinib, flavopiridol, and mitoxantrone. *J Pharmacol Exp Ther* 2010; 333: 788–796.

6. Colclough N, Chen K, Johnström P, et al. Building on the success of osimertinib: achieving CNS exposure in oncology drug discovery. *Drug Discov Today* 2019; 24: 1067–1073.

7. Varrone A, Varnas K, Jucaite A, et al. A PET study in healthy subjects of brain exposure of (11)C-labelled osimertinib – a drug intended for treatment of brain metastases in non-small cell lung cancer. *J Cereb Blood Flow Metab* 2020; 40: 799–807.

8. Kim M, Laramy JK, Mohammad AS, et al. Brain distribution of a panel of epidermal growth factor receptor inhibitors using cassette dosing in wild-type and Abcb1/Abcg2-deficient mice. *Drug Metab Dispos* 2019; 47: 393–404.

9. Agarwal S, Sane R, Oberoi R, et al. Delivery of molecularly targeted therapy to malignant glioma, a disease of the whole brain. *Expert Rev Mol Med* 2011; 13: e17.

10. van Tellingen O, Yetkin-Arik B, de Gooijer MC, et al. Overcoming the blood-brain tumor barrier for effective glioblastoma treatment. *Drug Resist Updat* 2015; 19: 1–12.

11. Szakács G, Paterson JK, Ludwig JA, et al. Targeting multidrug resistance in cancer. *Nat Rev Drug Discov* 2006; 5: 219–234.

12. Robey RW, Pluchino KM, Hall MD, et al. Revisiting the role of ABC transporters in multidrug-resistant cancer. *Nat Rev Cancer* 2018; 18: 452–464.

13. Kreisl WC, Bhatia R, Morse CL, et al. Increased permeability-glycoprotein inhibition at the human blood-brain barrier can be safely achieved by performing PET during peak plasma concentrations of tariquidar. *J Nucl Med* 2015; 56: 82–87.

14. Bauer M, Karch R, Zeitlinger M, et al. Approaching complete inhibition of P-glycoprotein at the human blood-brain barrier: an (R)-[^{11}C]verapamil PET study. *J Cereb Blood Flow Metab* 2015; 35: 743–746.

15. Bauer M, Römermann K, Karch R, et al. Pilot PET study to assess the functional interplay between ABCB1 and ABCG2 at the human blood-brain barrier. *Clin Pharmacol Ther* 2016; 100: 131–141.

16. Bauer M, Karch R, Wulkersdorfer B, et al. A proof-of-concept study to inhibit ABCG2- and ABCB1-mediated efflux transport at the human blood-brain barrier. *J Nucl Med* 2019; 60: 486–491.

17. Traxl A, Wanek T, Mairinger S, et al. Breast cancer resistance protein and P-glycoprotein influence in vivo disposition of ^{11}C-erlotinib. *J Nucl Med* 2015; 56: 1930–1936.

18. Tournier N, Goutal S, Auvity S, et al. Strategies to inhibit ABCB1- and ABCG2-mediated efflux transport of erlotinib at the blood-brain barrier: a PET study on non-human primates. *J Nucl Med* 2017; 58: 117–122.

19. Agarwal S, Manchanda P, Vogelbaum MA, et al. Function of the blood-brain barrier and restriction of drug delivery to invasive glioma cells: findings in an orthotopic rat xenograft model of glioma. *Drug Metab Dispos* 2013; 41: 33–39.

20. Verheijen RB, Yaqub MM, Sawicki E, et al. Molecular imaging of ABCB1/ABCG2 inhibition at the human blood brain barrier using elacridar and ^{11}C-erlotinib PET. *J Nucl Med* 2018; 59: 973–979.

21. Goutal S, Langer O, Auvity S, et al. Intravenous infusion for the controlled exposure to the dual ABCB1 and ABCG2 inhibitor elacridar in nonhuman primates. *Drug Deliv Transl Res* 2018; 8: 536–542.

22. Kreisl WC, Liow JS, Kimura N, et al. P-glycoprotein function at the blood-brain barrier in humans can be quantified with the substrate radiotracer ^{11}C-N-desmethyl-loperamide. *J Nucl Med* 2010; 51: 559–566.

23. Bauer M, Zeitlinger M, Karch R, et al. Pgp-mediated interaction between (R)-[^{11}C]verapamil and tariquidar at the human blood-brain barrier: a comparison with rat data. *Clin Pharmacol Ther* 2012; 91: 227–233.

24. Noguchi K, Kawahara H, Kaji A, et al. Substrate-dependent bidirectional modulation of P-glycoprotein-mediated drug resistance by erlotinib. *Cancer Sci* 2009; 100: 1701–1707.

25. Lee CA, O'Connor MA, Ritchie TK, et al. Breast cancer resistance protein (ABCG2) in clinical pharmacokinetics and drug interactions: practical recommendations for clinical victim and perpetrator drug-drug interaction study design. *Drug Metab Dispos* 2015; 43: 490–509.

26. Philippe C, Mairinger S, Pichler V, et al. Comparison of fully-automated radiosyntheses of [^{11}C]erlotinib for preclinical and clinical use starting from in target produced $^{11}C]CO_2$ or $[^{11}C]CH_4$. *EJNMMI Radiopharm Chem* 2018; 3: 8. [

27. Wanek T, Römermann K, Mairinger S, et al. Factors governing p-glycoprotein-mediated drug-drug interactions at the blood-brain barrier measured with positron emission tomography. *Mol Pharm* 2015; 12: 3214–3225.

28. Traxl A, Mairinger S, Filip T, et al. Inhibition of ABCB1 and ABCG2 at the mouse blood-brain barrier with marketed drugs to improve brain delivery of the model ABCB1/ABCG2 substrate [^{11}C]erlotinib. *Mol Pharm* 2019; 16: 1282–1293.

29. la Fougère C, Boning G, Bartmann H, et al. Uptake and binding of the serotonin 5-HT$_{1A}$ antagonist [^{18}F]-MPPF

in brain of rats: effects of the novel P-glycoprotein inhibitor tariquidar. *Neuroimage* 2010; 49: 1406–1415.

30. Kuntner C, Bankstahl JP, Bankstahl M, et al. Dose-response assessment of tariquidar and elacridar and regional quantification of P-glycoprotein inhibition at the rat blood-brain barrier using (R)-[^{11}C]verapamil PET. *Eur J Nucl Med Mol Imaging* 2010; 37: 942–953.

31. Loening AM and Gambhir SS. AMIDE: a free software tool for multimodality medical image analysis. *Mol Imaging* 2003; 2: 131–137.

32. Logan J, Fowler JS, Volkow ND, et al. Graphical analysis of reversible radioligand binding from time-activity measurements applied to [N-^{11}C-methyl]-(-)-cocaine PET studies in human subjects. *J Cereb Blood Flow Metab* 1990; 10: 740–747.

33. Auvity S, Caillé F, Marie S, et al. P-glycoprotein (ABCB1) inhibits the influx and increases the efflux of ^{11}C-metoclopramide across the blood-brain barrier: a PET study on non-human primates. *J Nucl Med* 2018; 59: 1609–1615.

34. Cui Y, Lotz R, Rapp H, et al. Muscle to brain partitioning as measure of transporter-mediated efflux at the rat blood-brain barrier and its implementation into compound optimization in drug discovery. *Pharmaceutics* 2019; 11: 595.

35. Lancaster MA, Renner M, Martin CA, et al. Cerebral organoids model human brain development and microcephaly. *Nature* 2013; 501: 373–379.

36. Randall EC, Emdal KB, Laramy JK, et al. Integrated mapping of pharmacokinetics and pharmacodynamics in a patient-derived xenograft model of glioblastoma. *Nat Commun* 2018; 9: 4904.

37. Goutal S, Gerstenmayer M, Auvity S, et al. Physical blood-brain barrier disruption induced by focused ultrasound does not overcome the transporter-mediated efflux of erlotinib. *J Control Release* 2018; 292: 210–220.

38. de Vries NA, Buckle T, Zhao J, et al. Restricted brain penetration of the tyrosine kinase inhibitor erlotinib due to the drug transporters P-gp and BCRP. *Invest New Drugs* 2012; 30: 443–449.

39. Bauer M, Matsuda A, Wulkersdorfer B, et al. Influence of OATPs on hepatic disposition of erlotinib measured with positron emission tomography. *Clin Pharmacol Ther* 2018; 104: 139–147.

40. Kamiie J, Ohtsuki S, Iwase R, et al. Quantitative atlas of membrane transporter proteins: development and application of a highly sensitive simultaneous LC/MS/MS method combined with novel in-silico peptide selection criteria. *Pharm Res* 2008; 25: 1469–1483.

41. Ito K, Uchida Y, Ohtsuki S, et al. Quantitative membrane protein expression at the blood-brain barrier of adult and younger cynomolgus monkeys. *J Pharm Sci* 2011; 100: 3939–39350.

42. Thiollier T, Wu C, Porras G, et al. Microdialysis in awake macaque monkeys for Central nervous system pharmacokinetics. *Animal Model Exp Med* 2018; 1: 314–321.

43. Feng B, Doran AC, Di L, et al. Prediction of human brain penetration of P-glycoprotein and breast cancer resistance protein substrates using in vitro transporter studies and animal models. *J Pharm Sci* 2018; 107: 2225–2235.

44. How J, Mann J, Laczniak AN, et al. Pulsatile erlotinib in EGFR-positive non-small-cell lung cancer patients with leptomeningeal and brain metastases: review of the literature. *Clin Lung Cancer* 2017; 18: 354–363.

45. Milton DT, Azzoli CG, Heelan RT, et al. A phase I/II study of weekly high-dose erlotinib in previously treated patients with nonsmall cell lung cancer. *Cancer* 2006; 107: 1034–1041.

46. Frohna P, Lu J, Eppler S, et al. Evaluation of the absolute oral bioavailability and bioequivalence of erlotinib, an inhibitor of the epidermal growth factor receptor tyrosine kinase, in a randomized, crossover study in healthy subjects. *J Clin Pharmacol* 2006; 46: 282–290.

47. Bankstahl JP, Bankstahl M, Römermann K, et al. Tariquidar and elacridar are dose-dependently transported by p-glycoprotein and bcrp at the blood-brain barrier: a small-animal positron emission tomography and in vitro study. *Drug Metab Dispos* 2013; 41: 754–762.

48. Wanek T, Kuntner C, Bankstahl JP, et al. A novel PET protocol for visualization of breast cancer resistance protein function at the blood-brain barrier. *J Cereb Blood Flow Metab* 2012; 32: 2002–2011.

49. Przystal JM, Waramit S, Pranjol MZI, et al. Efficacy of systemic temozolomide-activated phage-targeted gene therapy in human glioblastoma. *EMBO Mol Med* 2019; 11: e8492.

50. Pandey V, Ranjan N, Narne P, et al. Roscovitine effectively enhances antitumor activity of temozolomide in vitro and in vivo mediated by increased autophagy and caspase-3 dependent apoptosis. *Sci Rep* 2019; 9: 5012.